THE ASTROPHYSICAL JOURNAL, 243:345–368, 1981 January 15

OPTICAL AND INFRARED SPECTROPHOTOMETRY OF QUASI-STELLAR OBJECTS: THE SPECTRA OF 14 QSOs

R. C. PUETTER,[1] HARDING E. SMITH,[1] AND S. P. WILLNER[1]
Center for Astrophysics and Space Sciences, University of California, San Diego
AND
J. L. PIPHER[1]
Department of Physics and Astronomy, University of Rochester
Received 1980 May 16; accepted 1980 July 9

ABSTRACT

We present combined optical-infrared spectrophotometry of the emission line spectra of 14 QSOs. These observations allow determination of the Lα/Balmer ratios in high-redshift objects and the Pα/Balmer ratios in the low-redshift objects. An attempt is made to synthesize the "intrinsic" hydrogen line spectrum of QSOs. The resulting spectrum is inconsistent with optically thin recombination models reddened by dust, but agrees qualitatively with recent optically thick calculations with $T_e \gtrsim 1.5\times10^4$ K in the line emitting region with perhaps a small amount of reddening [$E(B-V)\lesssim0.2$]. Much of the observed "continuum" structure can be attributed to optically thin Balmer continuum emission from a region with $T_e \lesssim 10^4$ K plus blended optically thick Fe II transitions.

Subject headings: infrared: spectra — quasars — spectrophotometry

I. INTRODUCTION

Since the discovery of quasi-stellar objects, considerable activity has been directed at understanding the nature of the QSO energy source and emission. It is now thought that the observed emission arises from three physically distinct regions. The "central machine" with dimensions on the order of 0.1 pc is at the heart of the QSO. This object produces the (presumably) nonthermal continuum which in turn excites nearby gas. The second region surrounds the central source and is believed to contain dense ($n_H \approx 10^9$ cm^{-3}) condensations that produce broad permitted lines. The widths of these lines are normally attributed to motions of the emission line clouds with relative velocities approaching 0.1c. A third, lower density ($n_H \lesssim 10^6$ cm^{-3}) region is believed to surround or be mixed with the broad line clouds, producing the narrow forbidden lines and, in some cases, narrow permitted line components. Recently, there has been renewed interest in the broad line region due to Baldwin's (1977) suggestion that the Lα/Hβ ratio is about a factor of 10 smaller than predicted by case B recombination theory and Grasdalen's (1976) observation that case B line ratios with conventional reddening by dust are unable to reproduce the combined Pα/Hβ ratio and Balmer decrement in 3C 273.

The problem of investigating QSO hydrogen emission naturally divides itself into two regimes: combined UV-optical observations and combined optical-IR observations. UV-optical observations allow measurement of Lα/Hα in low redshift QSOs ($z \lesssim 0.3$), and optical-IR observations in high-redshift QSOs ($2.0 \lesssim z \lesssim 2.8$). There have already been several measurements of this ratio. Working in the optical and infrared, Hyland, Becklin, and Neugebauer (1978), Soifer *et al.* (1979), and Puetter, Smith, and Willner (1979) have reported values for the Lα/Hα ratio in two high-redshift QSOs. In the UV, Davidsen, Hartig, and Fastie (1977) and Baldwin *et al.* (1978) have measured Lα in two more low-redshift QSOs. All of these observations seem to confirm Baldwin's suggestion that Lα/Hβ≈3 to within a factor of about 2. More recently, a number of observations of Lα in Seyfert galaxies and N systems have become available through observations with the *International Ultraviolet Explorer*. These observations also show the low Lα/Balmer broad line ratio.

The first theoretical attempts at explaining the Lα/Balmer ratio suggested that the Lα flux was suppressed below the case B recombination value by extinction due to dust. Subsequent investigations realized the possible importance of collisional excitation and radiative transfer effects in determining the line ratios (cf. Netzer 1975; Baldwin and Netzer 1978; Hyland,

[1]Visiting Astronomers at Kitt Peak National Observatory and Cerro Tololo Inter-American Observatory which are operated by the Association of Universities for Research in Astronomy under contract with the National Science Foundation.

Becklin, and Neugebauer 1978; Krolik and McKee 1978; Puetter *et al.* 1978; Kwan and Krolik 1979; Ferland and Netzer 1979; Shuder and MacAlpine 1979; Netzer and Davidson 1979; Puetter *et al.* 1979; Mathews, Blumenthal, and Grandi 1980; Canfield and Puetter 1980, 1981*b*). Reddening by dust is also a possible explanation of the steep Balmer decrements (Baldwin 1975). Recent UV observations of the active radio galaxy 3C 390.3 by Ferland *et al.* (1979), however, suggest that effects other than reddening may dominate the observed line ratios. In this object both broad and narrow hydrogen line components are observed. The narrow components are observed to be in the case B line ratios, but the broad line components show a depressed $L\alpha/H\beta$ ratio. Thus Ferland *et al.* conclude that external reddening cannot explain the reduced broad line $L\alpha$/Balmer ratio, at least in this object.

An observational approach to resolving the problem of the relative importance of reddening is to observe $P\alpha$ in the near-infrared and the Balmer lines in the optical in low-redshift QSOs ($0.1 \lesssim z \lesssim 0.3$). Grasdalen's (1976) initial measurement of $P\alpha$ in 3C 273 suggested that case B recombination plus dust extinction like that of our Galaxy could not explain both the steep Balmer decrement and the $P\alpha/H\beta$ ratio in that object. This conclusion has been confirmed by Puetter *et al.* (1978) for that object and also for the quasar PG 0026+129.

In order to define more clearly the relative effects of dust, either internal or external to the line emitting region, radiation transfer, and other effects, we have begun an extensive program of optical and infrared spectrophotometry of QSOs. Below we present observations of Paschen/Balmer line ratios in low-z QSOs and also $L\alpha/H\alpha$ observations in three high-redshift QSOs. These observations will be discussed in terms of current theoretical models for QSO broad emission line regions.

II. THE OBSERVATIONS

The optical observations reported here, as well as most of the infrared observations, were made with the 3m Shane telescope of Lick Observatory. Additional infrared observations were obtained using the 4 m telescopes of Cerro Tololo Inter-American Observatory and Kitt Peak National Observatory. Table 1 gives the sample of objects and a journal of observations for the optical and infrared data presented here.

a) *Infrared Observations*

Most of the infrared observations reported here were made using a UCSD InSb spectrometer, which employs a circular variable filter wheel with resolution $\Delta\lambda/\lambda \approx 0.035$, covering the region from 1.6 to 3.0 μm. Broad band measurements from 1.25 to 2.28 μm and occasionally 3.5 μm were obtained. At KPNO and CTIO some of the observations were made with "in house" InSb systems with a resolution $\Delta\lambda/\lambda \approx 0.015$. In addition, a few observations were made with the UCSD system employing a $\Delta\lambda/\lambda \approx 0.02$ wheel. Observations made at KPNO or CTIO, or with resolution other than 0.035 are noted in Table 1. The angular diameter of the beam on the sky for these observations was 7.″0–7.″5. The system response and atmospheric extinction generally were calibrated using A-type (except as noted in the Appendix) stars as standards. These stars were assumed to have roughly 9700 K blackbody energy distributions and fluxes consistent with the calibration of Vega by Oke and Schild (1970). The absolute magnitudes of the standards used are probably accurate to a few percent except as noted in the Appendix.

Line intensities were derived by making χ^2 minimization fits to the infrared data, assuming that the continuum may be approximated as a power law and that the line may be represented by the convolution of two triangles of arbitrary height but previously determined width. To a good approximation the transmission of the filter wheel is triangular with a full width at half-maximum of 3.5% of the central wavelength. The shape of the line itself was approximated by a second triangle with a FWHM (velocity) determined from hydrogen lines observed at optical wavelengths. While one would prefer to determine the line width directly from the infrared data, the resolution of the filter wheel and the relatively poor signal-to-noise of our observations do not justify doing so. For objects for which good data exist, the permitted lines do appear to have the same profiles (e.g., Baldwin and Netzer 1978) so that we do not expect to introduce significant errors by assuming that the optical and infrared features have the same velocity widths. The error introduced by the assumption of a triangular line profile may be judged from the optical data shown in Figure 1 and is believed to be small compared with other errors. Figure 1 also shows the infrared data along with the line and continuum from a typical χ^2 fit.

The statistical uncertainty in the determination of the height above the continuum of the line (and hence the line flux) was determined from the variance of the height as determined by the χ^2 minimization procedure. The statistical uncertainty, of course, says nothing about the errors introduced by systematic effects. To attempt to evaluate the magnitude of systematic errors, we performed a grid of χ^2 fits for each line, changing various parameters within what we considered to be reasonable limits. In some cases, we included more or fewer narrow-band and/or broad-band points to determine the continuum. In other cases we assumed that the continuum flux per Hertz was linear as a function of λ while in others we assumed F_λ was linear in λ. After several χ^2 fits were completed, we calculated an average value of the line flux. This value,

TABLE 1

JOURNAL OF OBSERVATIONS

QSO	z	UT DATE OF OBSERVATION[a] Blue	Yellow	Red	IR
III Zw 2	0.089	8/2/79	*10/4/78*	*10/3/78*	9/20/78
					9/22/78
					12/15/78
PG 0026+129.....	0.147	*10/11/77*	*10/11/77*	*8/11/78*	10/28/77[b,c]
		11/14/77	*8/12/78*	*8/12/78*	11/29/78
				10/3/78	
PHL 957.....	2.69	*10/9/77*	8/12/78	...	12/1/77[d]
		11/14/77	...	...	9/20/78
					9/22/78
NAB 0205+024...	0.155	*11/14/77*	*10/12/77*	*8/11/78*	9/20/78
					12/14/78
PKS 0837−120....	0.200	...	...	...	4/6/79[c,e]
Q1101−264.....	2.145	...	...	...	4/6/79
B2 1128+315	0.289	...	...	...	4/28/78[b,c]
B2 1225+317	2.20	4/20/77	4/19/77	...	3/19/78[d]
		5/21/77	3/7/78		
3C 273	0.158	5/26/73	6/3/73	*2/4/79*	4/28/78[b,c]
		2/5/79	3/7/78		
			2/5/79		
Ton 256	0.131	*5/3/79*	*7/1/78*	*8/12/78*	7/22/78
		5/4/79	*8/12/78*	*7/9/79*	7/23/78
			8/11/78		
V396 Her.....	...	*5/27/79*	*4/21/79*	4/22/79	
PKS 2135−147....	0.200	*8/17/79*	*10/4/78*	*10/2/78*	9/20/78
				10/3/78	
2141+174.....	0.213	*10/11/77*	*10/11/77*	*10/12/77*	7/21/78
		11/13/77	10/12/77	8/11/78	7/22/78
		11/14/77	*8/2/79*		7/23/78
					7/24/78
4C 31.63.....	0.297	*7/18/77*	*10/10/77*	*10/12/77*	7/21/78
		7/19/77	*10/12/77*	*8/11/78*	7/22/78
			6/30/78		7/23/78
					7/24/78
					7/12/79
					7/13/79
					7/14/79

[a] Dates which are italic indicate nights on which large aperture data were taken in addition to small aperture data.
[b] KPNO 4 m observation.
[c] Resolution = 1.5%.
[d] Resolution = 2.0% UCSD system.
[e] CTIO 4 m observation.

along with the typical statistical uncertainty from the χ^2 fits and the dispersion among the different fits (i.e., the standard deviation of the values of the line flux), is reported in Table 2. The statistical uncertainty reflects the quality of the data, and should be used, for example, in deciding such questions as whether or not a line has been detected. The model dispersion reflects the applicability of the model of the line and continuum to the data. The uncertainty in the absolute determination of the line flux should be some combination of these two uncertainties (we have taken it to be the square root of the sum of the squares).

b) Optical Observations

The optical observations reported here were made with the Robinson-Wampler image dissector scanner on the Lick Observatory Shane telescope. With the gratings employed for these observations the IDS has a resolution of 10 Å (FWHM) and covers approximately 2400 Å of spectrum. Three settings are therefore necessary to cover the entire wavelength range over which the IDS is sensitive (3000 Å$\lesssim\lambda\lesssim$8800 Å) with reasonable overlap. Because the aperture best matched to the resolution of the image tube/dissector chain is small

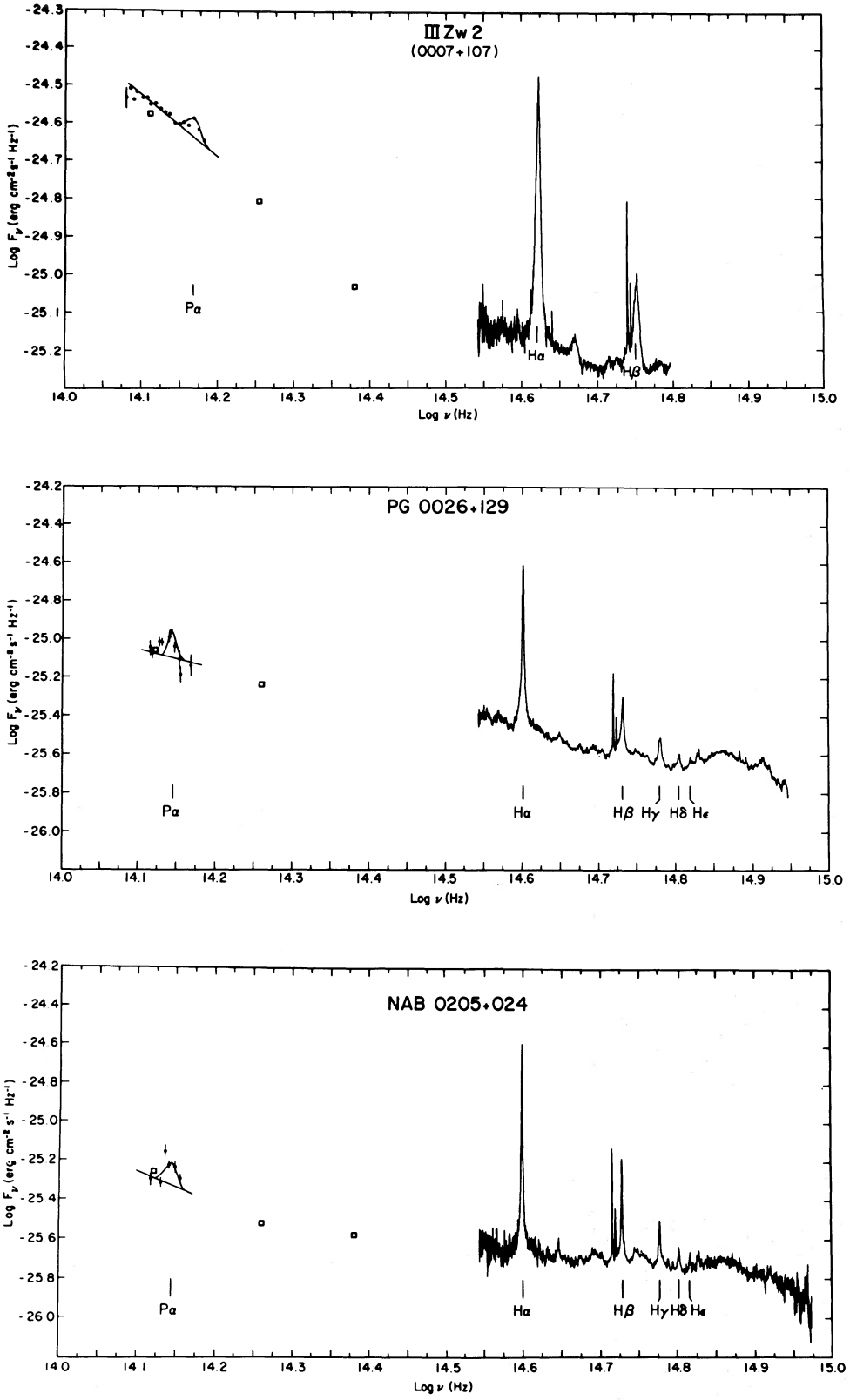

FIG. 1.—Optical and infrared spectrophotometry of the objects in our program normalized to the calibration of Vega by Oke and Schild (1970). The spectral resolution of the optical data is 10 A. The spectral resolution of the infrared data varies between $\Delta\lambda/\lambda=0.015$ and 0.035 but is typically 0.035. Also plotted are broad band infrared measurements (□) and a typical χ^2 fit to the infrared emission line. The bandpasses of the infrared broad-band filters are 0.3, 0.3, and 0.5 μm for the 1.25, 1.65, and 2.28 μm filters, respectively.

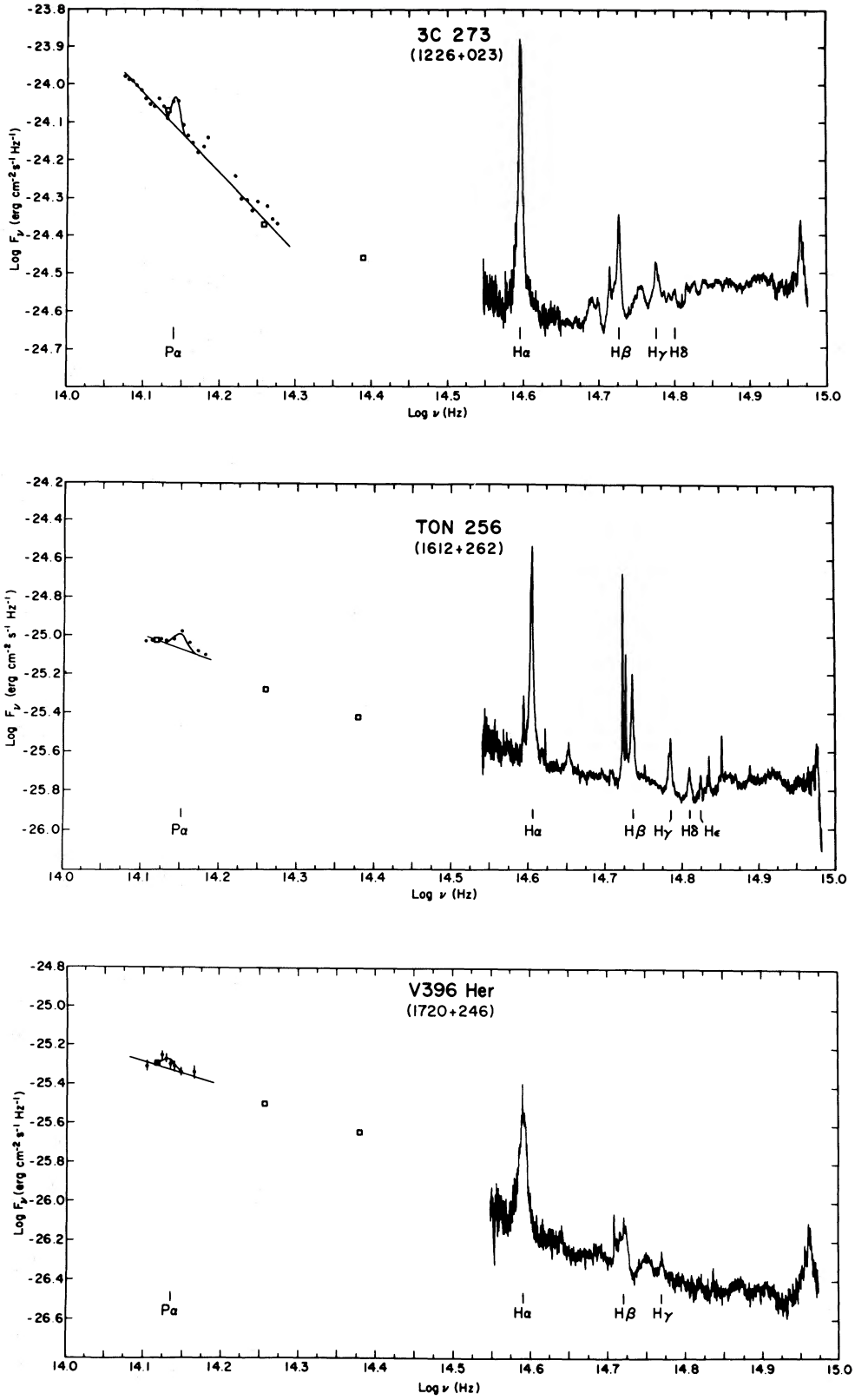

FIG. 1.—*Continued*

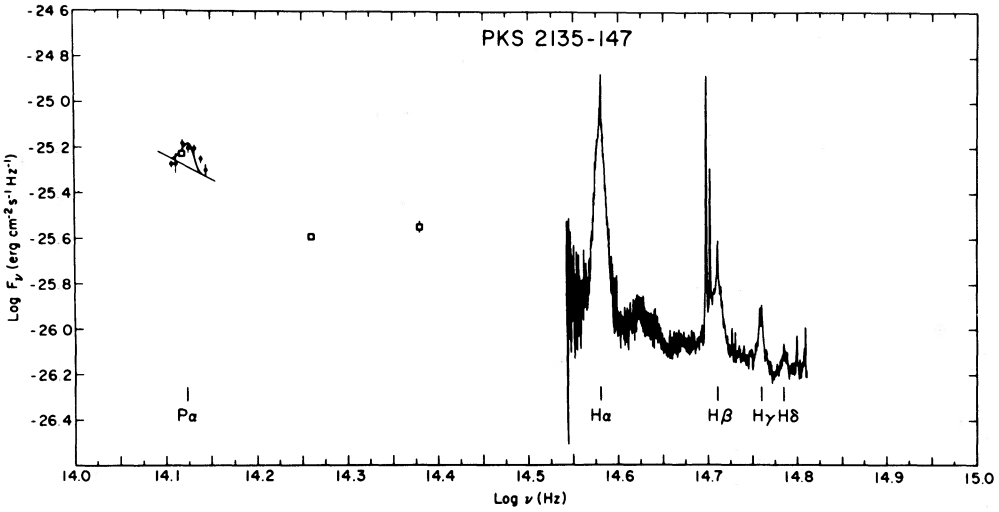

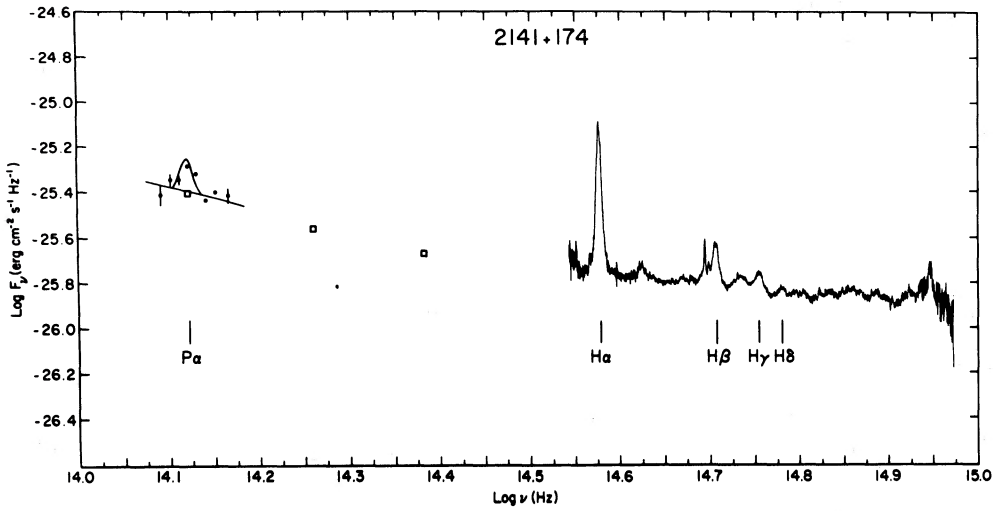

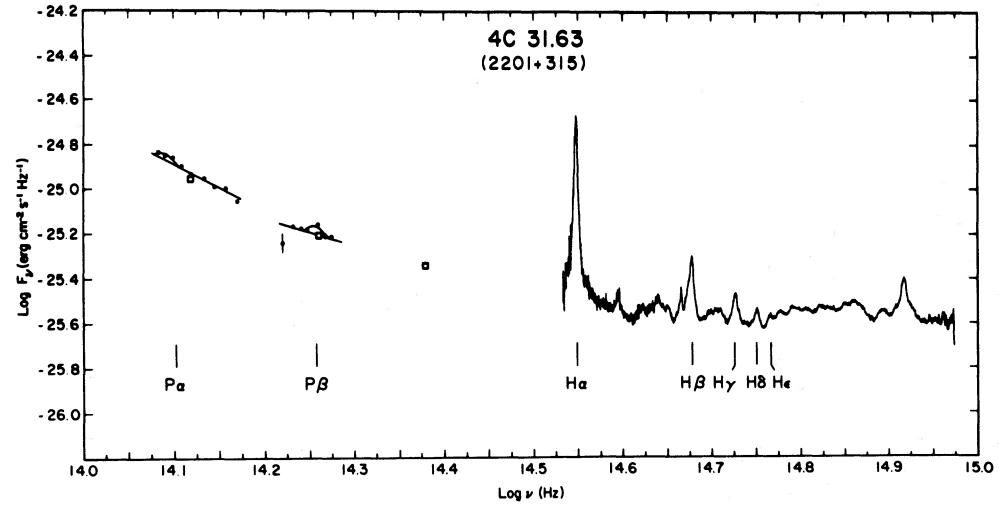

FIG. 1.—*Continued*

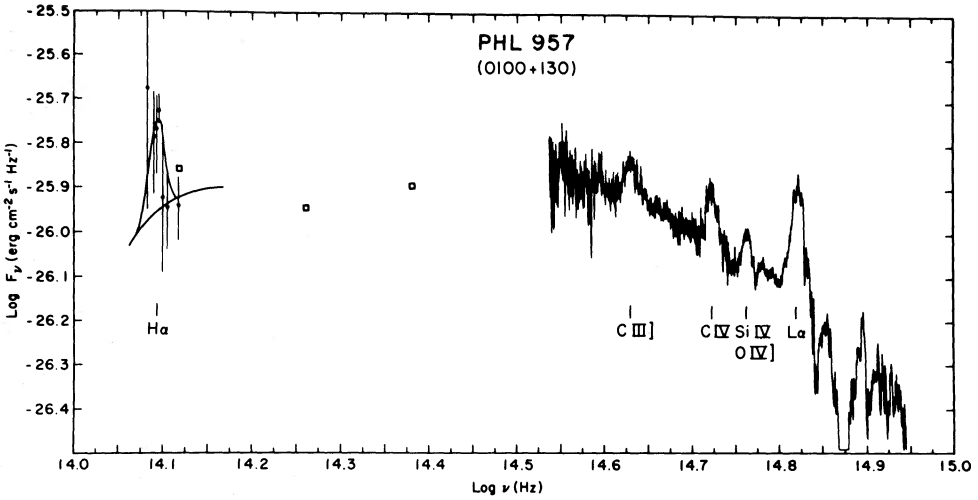

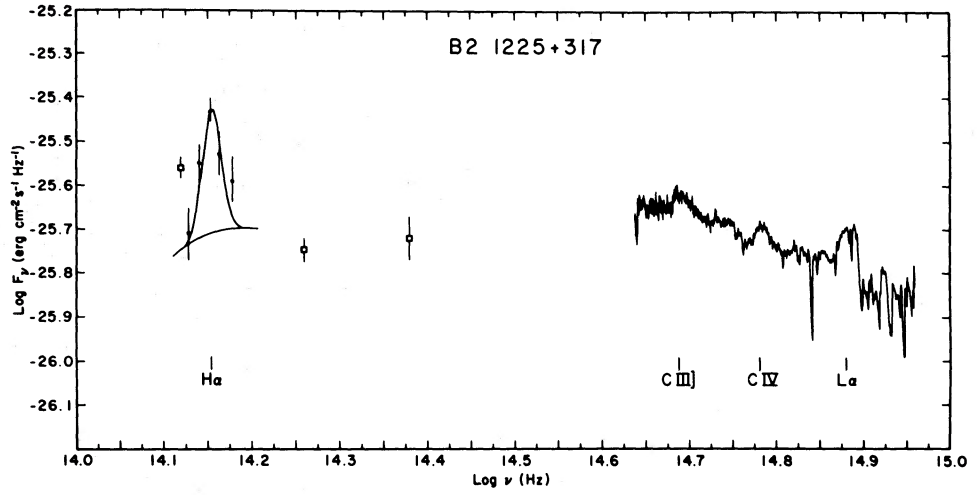

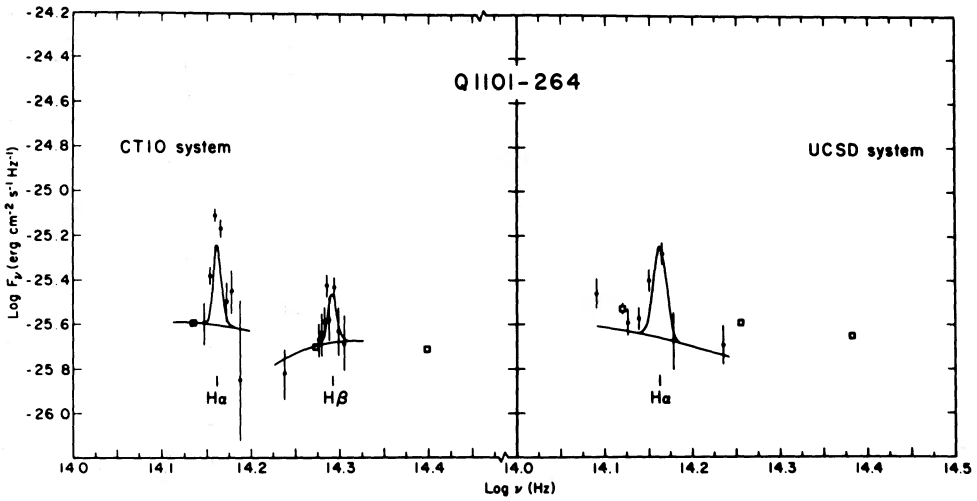

FIG. 1.—*Continued*

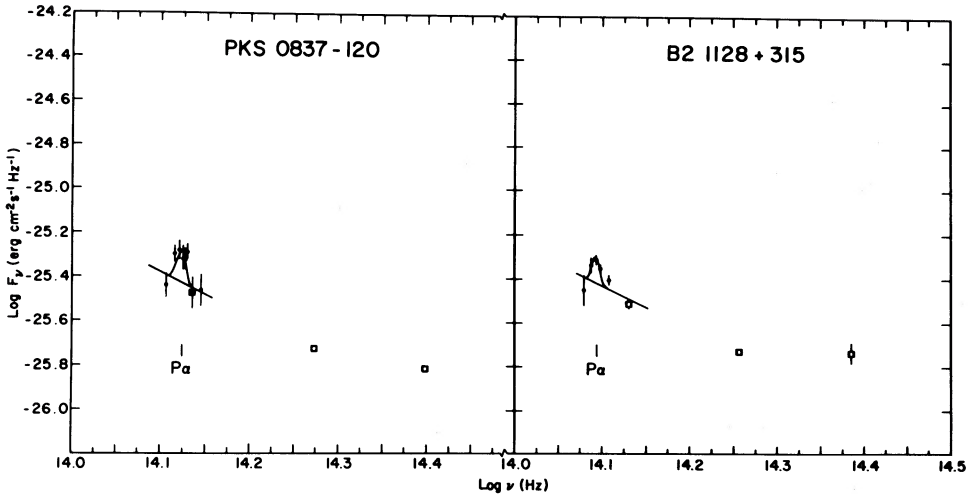

FIG. 1.—*Continued*

(~2.″8), accompanying observations with a larger aperture (generally 8″) were made in order to obtain absolute spectrophotometry. Standard photometric procedures were employed to reduce the observations to incident flux above the Earth's atmosphere (see, for example, Smith 1975; Baldwin 1975).

It was our goal to obtain two observations, each accompanied by a large aperture observation, at each wavelength setting—blue, yellow, red. As can be seen from Table 1, this goal has not been achieved for the majority of objects.

The observations are summed by a routine which normalizes the overlapping wavelength regions of adjacent scans to produce the spectra shown in Figure 1. In some cases the observations are separated by several months so that variability in the continuum could produce errors in the line intensities due to this normalization procedure. Two of the objects discussed here, III Zw 2 and PKS 2135−147, exhibited significant variability during this period. Fortunately, the Pα and Balmer measurements were obtained within a few weeks of each other in both cases. The overlapping con-

TABLE 2

INFRARED BROAD-BAND AND LINE OBSERVATIONS

OBJECT	F_ν^{cont} [a]				LINE [b]			
	1.25 μm	1.65 μm	2.28 μm	3.5 μm	$F_{\text{obs}}^{\text{line}}$	σ_{stat}	σ_{model} (%)	σ_T
Pα Observations								
III Zw2	9.2	15.4	26.4	51.2	1.0	32	6	33
PG 0026+129	...	6.0	8.7	...	1.2	15	10	18
NAB0205+024	2.7	3.0	5.5	...	0.65	25	7	26
PKS 0837−120	1.7	1.9	2.2	...	0.33	34	14	37
B2 1128+315	1.9	1.8	3.4	...	0.30	29	28	40
3C 273	31.4	41.6	96.4	...	5.0	31	9	32
Ton 256	3.9	5.3	10.7	15.0 (3σ)	0.95	15	8	17
V396 Her	2.3	3.2	5.2	...	0.28	39	30	49
PKS 2135−147	2.8	2.5	5.9	...	0.69	20	6	21
2141+174	2.1	2.8	4.0	...	0.72	19	14	24
4C 31.63	4.6	6.2	11.3	...	0.47	38	11	40
(Pβ)	...	...	...	...	0.39	29	3	29
Hα Observations								
PHL 957	1.3	1.1	1.4	...	0.61	26	8	27
Q1101−264	2.2	2.9	3.0	...	2.0	18	7	19
(Hβ)	...	...	...	...	0.73	29	16	33
B2 1225+317	1.9	1.8	2.2	...	1.1	18	11	21

[a] Continuum fluxes in units of 10^{-26} ergs cm^{-2}s^{-1}Hz^{-1}.
[b] Line fluxes in units of 10^{-13} ergs cm^{-2}s^{-1}.

tinuum measures for the other large-aperture observations generally agree to a few percent. The spectra shown in Figure 1 have been normalized to the large-aperture fluxes. This normalization has two parts: a gray shift, typically 30% but for some objects, nearly up to a factor of 2, which corrects for light spilling out of the 2.″8 aperture, and a wavelength-dependent correction for atmospheric dispersion. All observations were made at small hour angles; even so, refraction of the blue and UV, combined with the red (S-25) response of the TV guiding system at Lick led to the necessity of applying corrections up to 30% at the blue end of the spectrum in some cases. These corrections, however, do not significantly influence the hydrogen line ratios which are the heart of this work. For objects in common with the study of Neugebauer *et al.* (1979) our measures are in good agreement, and in most cases we believe that systematic photometric errors should not exceed 10%.

Line intensities were derived by a program which fits least squares polynomials (linear or quadratic) through preselected continuum intervals, subtracts the interpolated continuum, and integrates over the line interval. This technique is necessarily quite sensitive to the choice of continuum interval, and we believe that this is the largest source of uncertainty in the quoted line intensities. As one may see in Figure 1, most of these QSOs have very rich emission line spectra; real continuum intervals are difficult to find, and line blending further disguises the true continuum level. Spectrophotometry of several of these objects has previously been published by Baldwin (1975) or by Neugebauer *et al.* (1979). Because of our high signal-to-noise and resolution, we expect that the quality of the line intensity measurements reported here to be generally higher than previously reported values. In cases where we do not have good spectrophotometry, we have adopted line intensities from these sources.

For many objects in this sample, strong telluric O_2 and H_2O absorption overlie Hα or other features of interest. This absorption does not follow normal atmospheric extinction corrections and may be variable during the course of a night. For most red observations, accompanying observations of a star nearby were obtained and the atmospheric absorption removed by dividing the QSO spectrum by the normalized stellar spectrum over the region covered by these bands. For a few observations, it was necessary to divide by the spectrum of a standard star observed at the beginning of the night. The 7600 Å band of O_2 is particularly strong and lies within the Hα profiles for PG 0026+129, NAB 0205+024, 3C 273, V396 Her, and PKS 2135−147; thus this is a very important correction, up to 30% for the worst case.

The combined optical/infrared line ratios are given in Tables 3 and 4 along with relevant UV measures of Lα when available. In order to estimate the extinction due to material in the Galaxy, we have employed the correlation, found by Burstein and Heiles (1978), between $E(B-V)$, 21 cm hydrogen column density, and Shane-Wirtanen (1967) galaxy counts to calculate the galactic reddening in the direction of each of the objects in our sample. The line ratios were then dereddened using the mean galactic extinction curve given by Savage and Mathis (1979). These corrected line ratios are also given in the tables. Since these objects are at relatively high galactic latitudes, the corrections are small; only for 4C 31.63 does the color excess due to galactic reddening exceed 0.1.

c) *Notes on Individual Objects*

i) *III Zw 2*

This object, classified variously as a QSO or a Seyfert 1 galaxy, has been suggested to be variable by up to several tenths of a magnitude (Green 1976; Rieke and Lebofsky 1979). Our continuum measures show that III Zw 2 was about 40% brighter in the fall of 1978 than in 1977 July (Neugebaur *et al.* 1979). The data reported here were all obtained within a span of a few weeks, so we do not expect that variability should be a serious source of error.

Osterbrock (1977) has also observed the spectrum of III Zw 2. He finds a Balmer decrement Hα/Hβ=3.68, steeper than our value of 3.34 but within the observational error.

ii) *PG 0026+129*

Preliminary results for this object were published by Puetter *et al.* (1978). The χ^2 fitting procedure for Pα and additional optical spectrophotometry have caused slight revisions in the line ratios, but the essential conclusions of that paper—that the hydrogen line spectrum of PG 0026+129 cannot be reproduced by case B ratios reddened by a physically realistic extinction curve—remain valid.

iii) *PHL 957*

Our Lα intensity is in good agreement with that determined by Lowrance *et al.* (1972) and Baldwin and Netzer (1978).

iv) *B2 1128+315*

Unfortunately, optical spectrophotometric measures of this object do not yet exist.

v) *B2 1225+317*

Previous optical/infrared spectrophotometry have been reported by Puetter, Smith, and Willner (1979) and Soifer *et al.* (1979). The revised line fitting procedure has brought our Hα intensity into closer agreement with the value obtained by Soifer *et al.*

TABLE 3

LINE INTENSITY RATIOS FOR LOW-z OBJECTS

		III Zw 2			PG 0026+129			NAB 0205+024			PKS 0837−120[a]		
		$\frac{F_\lambda}{F_{H\beta}}$	$\left(\frac{F_\lambda}{F_{H\beta}}\right)_{corr}$	W_λ^{rest} (Å)	$\frac{F_\lambda}{F_{H\beta}}$	$\left(\frac{F_\lambda}{F_{H\beta}}\right)_{corr}$	W_λ^{rest} (Å)	$\frac{F_\lambda}{F_{H\beta}}$	$\left(\frac{F_\lambda}{F_{H\beta}}\right)_{corr}$	W_λ^{rest} (Å)	$\frac{F_\lambda}{F_{H\beta}}$	$\left(\frac{F_\lambda}{F_{H\beta}}\right)_{corr}$	W_λ^{rest} (Å)
LINE	λ(Å)	$E_{B-V}=0.048$			$E_{B-V}=0.036$			$E_{B-V}=0.019$			$E_{B-V}=0.061$		
Lα	1216	...	...	...	5.0	6.0	...	...	...	...	...	...	...
Bc[b]	...	...	...	...	2.9	3.0	...	3.4	3.5	...	...	...	...
Mg II	2799	...	...	...	...	...	...	...	...	...	...	...	...
[Ne V]	3426	...	...	...	0.04	0.04	1	...	...	...	...	...	...
[O II]	3727	...	...	...	0.02	0.02	0.5	...	...	...	...	...	...
He I [Ne III]	3868 3869	...	...	...	0.03	0.03	1	...	...	...	...	...	...
[Ne III] Hϵ	3968 3970	...	...	...	0.04	0.04	1	0.06	0.06	3	...	...	...
Hδ	4340	...	...	...	0.12	0.12	7	0.15	0.15	10	...	...	...
Hγ	4340	...	...	...	0.33	0.34	21	0.48	0.48	35	0.35	0.36	30
[O III]	4363	...	...	...	0.10	0.10	6	0.03	0.03	2	...	...	...
Hβ	4861	1.00	1.00	75	1.00	1.00	77	1.00	1.00	87	1.00	1.00	105
[O III]	4959 5007	0.34	0.34	23	0.35	0.35	26	0.51	0.51	44	0.82	0.82	90
He I	5876	0.14	0.14	15	0.06	0.06	5	0.08	0.08	10	...	...	...
Hα	6563	3.34	3.19	375	3.38	3.27	325	3.10	3.05	410	4.32	4.09	540
[N II]	6584	...	...	...	...	...	...	...	...	...	...	...	...
Pβ	12818	...	...	...	...	...	...	...	...	...	...	...	...
Pα	18751	0.26	0.23	...	0.61	0.55	...	0.36	0.34	...	0.48	0.41	...
$F_{H\beta}^{obs}$ (10^{-13} ergs cm^{-2} s^{-1})		4.8	5.5	...	2.0	2.2	...	1.8	1.9	...	0.7	...	...

TABLE 3—*Continued*

		3C 273			Ton 256			V396 Her		
		$\frac{F_\lambda}{F_{H\beta}}$	$\left(\frac{F_\lambda}{F_{H\beta}}\right)_{corr}$	W_λ^{rest} (Å)	$\frac{F_\lambda}{F_{H\beta}}$	$\left(\frac{F_\lambda}{F_{H\beta}}\right)_{corr}$	W_λ^{rest} (Å)	$\frac{F_\lambda}{F_{H\beta}}$	$\left(\frac{F_\lambda}{F_{H\beta}}\right)_{corr}$	W_λ^{rest} (Å)
LINE	λ(Å)	$E_{B-V}=0.010$			$E_{B-V}=0.026$			$E_{B-V}=0.072$		
Lα	1216	5.3	5.6	...	...	...	...	...	...	...
Bc	...	6.0	6.1	...	1.7	1.8	...	≲2.7	≲2.9	...
Mg II	2799	...	...	...	...	...	...	2.0	2.3	65
[Ne V]	3426	...	...	...	0.03	0.03	3	...	...	...
[O II]	3727	...	...	...	0.10	0.10	9	0.05	0.05	3
He I	3868	...	...	...	0.06	0.06	6	...	...	...
[Ne III]	3869									
[Ne III]	3968	...	...	...	0.05	0.05	6	...	...	...
Hε	3970									
Hδ	4101	...	...	...	0.14	0.14	18	...	...	...
Hγ	4340	0.43	0.43	25	0.28	0.29	36	0.19b	0.20b	12.5
								0.04n	0.04n	2.5
[O III]	4363	...	...	...	0.01	0.01	1.5	...	...	...
Hβ	4861	1.00	1.00	82	1.00	1.00	140	0.94b	0.94b	68
								0.06n	0.06n	5
[O III]	4959	...	...	...	...	1.09	150	0.17	0.17	12
	5007									
He I	5876	...	...	...	...	...	...	0.12	0.12	10
Hα	6563	2.87	2.84	386	3.07	3.00	625	5.26b	4.92b	430
								0.36n	0.34n	30
[N II]	6584	...	...	...	0.20	0.19	40	...	...	...
Pβ	12818	...	...	...	...	...	...	...	...	...
Pα	18751	0.22	0.22	...	0.34	0.32	...	0.74	0.63	...
$F_{H\beta}^{obs}(10^{-13}$ ergs cm^{-2}s^{-1})		21.6	22.2	...	2.8	3.0	...	0.38	0.46	...

TABLE 3—*Continued*

		PKS 2135-147			2141+174			4 C31.63		
LINE	λ(Å)	$\frac{F_\lambda}{F_{H\beta}}$	$\left(\frac{F_\lambda}{F_{H\beta}}\right)_{corr}$	W_λ^{rest} (Å)	$\frac{F_\lambda}{F_{H\beta}}$	$\left(\frac{F_\lambda}{F_{H\beta}}\right)_{corr}$	W_λ^{rest} (Å)	$\frac{F_\lambda}{F_{H\beta}}$	$\left(\frac{F_\lambda}{F_{H\beta}}\right)_{corr}$	W_λ^{rest} (Å)
		$E_{B-V}=0.042$			$E_{B-V}=0.105$			$E_{B-V}=0.128$		
Lα	1216	...	...	...	...	...	...	...	...	...
Bc		...	...	...	≲2.4	≲2.7	...	4.3	4.9	...
Mg II	2799	...	...	...	1.4	1.7	35	1.6	2.1	37
[Ne V]	3426	...	...	...	...	...	...	...	...	...
[O II]	3727	...	...	...	...	...	...	...	...	...
He I + [Ne III]	3868 + 3869	...	...	...	...	...	...	...	...	...
[Ne III] + Hε	3968 + 3970	0.04	0.04	5	0.13	0.14	7	...	...	...
Hδ	4101	0.08	0.08	12	0.15	0.16	8	0.18	0.19	11
Hγ	4340	0.27b 0.02n	0.27b 0.02n	45b 3n	0.49	0.51	30	0.38	0.40	21
[O III]	4363	0.02	0.02	3	...	...	...	...	...	...
Hβ	4861	0.93b 0.07n	0.93b 0.07n	166b 12n	1.00	1.00	75	1.00	1.00	70
[O III]	4959 + 5007	1.21	1.21	215	0.17	0.17	10	...	...	...
He I	5876	...	...	...	0.2:	0.2:	17:	...	...	...
Hα	6563	4.85b 0.39n	4.67 0.38n	1050b 93n	3.20	2.91	330	4.90	4.40	510
[N II]	6584	...	...	...	...	...	...	...	...	...
Pβ	12818	...	...	...	...	...	...	0.22	0.17	...
Pα	18751	0.21	0.19	...	0.72	0.55	...	0.25	0.18	...
$F_{H\beta}^{obs}(10^{-13}$ ergs cm^{-2}s^{-1})		1.5	1.7	...	1.0	1.3	...	1.9	2.6	...

[a] Optical data from Neugebauer *et al.* 1979.
[b] Bc = Balmer continuum.

vi) *3C 273*

Line intensities for 3C 273 have been reported by several authors (Baldwin 1975; Neugebauer *et al.* 1979; Boksenberg *et al.* 1975) with reported Hα/Hβ ratios varying from 2.8 to 5.2. 3C 273 is not among the highly variable QSOs, and we suspect that these differences represent the error in the determination of the line ratio rather than variability in the emission lines. Our value falls at the lower end of the range.

vii) *V396 Herculis*

This object and PKS 2135−147 show distinct broad and narrow components to the Balmer line profiles. We have crudely deconvolved the lines into broad and narrow components. Because of our poorer resolution in the infrared, we are unable to separate the components of Pα; thus the ratios reported here are for the sum of the two components. In at least one object, 3C 390.3 (Ferland *et al.* 1979) the narrow components exhibit "normal" (case B) ratios while the broad lines exhibit "anomalous" ratios similar to the broad lines in other objects. Since the narrow components in V396 Her and 2135−147 are only a few percent of the total intensity, the ratios quoted here most nearly reflect the broad component.

viii) *PKS 2135−147*

The broad components in PKS 2135−147 are exceedingly wide with full widths at zero intensity corresponding to a velocity width of nearly 25,000 km $s.^{-1}$.

PKS 2135−147 has also been observed by Baldwin (1975) who finds much smaller equivalent widths. We suspect that this difference is due to variability in the continuum. Our blue scan, obtained nearly a year after the other optical data shows that the continuum had brightened by about 30% over that time interval. The line intensities reported here were all obtained within a 2 week period in 1978 September-October.

ix) *2141+174 (=OX 169)*

The spectrum of this object lends additional support to our conclusion that the broad line emitting region is optically thick. The Balmer emission profiles in 2141+174 are self-reversed, possibly due to absorption due to the presence of an emission-line cloud along the line of sight (Smith 1980). The inferred optical depth in Hα is at least $\tau = 40$.

x) *4C 31.63*

This object shows unusually strong Fe II emission as one can see in Figures 1 and 6. We discuss the Fe II spectrum of 4C 31.63 in more detail in § III *c*. With the redshift of 4C 31.63, Pα lies right at the edge of the 2.3 μm window so that this line intensity is particularly uncertain. Previous optical observations of this object have also been reported by Grandi and Phillips (1979).

The QSO 4C 31.63 is the lowest galactic latitude object in this survey ($b^{II} = -19°$) and shows Galactic H and K absorption with $W_\lambda(K) \approx 1$ Å, similar to the interstellar line strengths present in the spectrum of 3C 273, $W_\lambda(K) = 0.5$ Å (Greenstein 1968), and horizontal branch stars in some globular clusters (Sargent 1967; Greenstein 1968).

III. DISCUSSION

a) The Hydrogen Line Spectrum

Probably the most striking recent result concerning QSO broad line spectra is the unexpectedly low Lα/Balmer line ratio. In Figure 2 we plot the Lα/Hα ratios versus the Hβ/Hα ratios for the three high-redshift QSOs in our infrared-optical sample, as well as for other broad line objects which have published Lα/Hα/Hβ intensities. Our results confirm that the Lα/Hα ratio in the broad line region is depressed by a factor of between 5–20 below the value of about 12 expected for a case B recombination (see, for example,

TABLE 4

LINE INTENSITY RATIOS FOR HIGH-*z* OBJECTS

LINE		PHL 957 $E(B-V)=0.03$		Q1101–264[a] $E(B-V)=0.03$		B2 1225+317[b] $E(B-V)=0.00$	
		$F_\lambda/F_{H\alpha}$	$(F_\lambda/F_{H\alpha})_{corr}$	$F_\lambda/F_{H\alpha}$	$(F_\lambda/F_{H\alpha})_{corr}$	$F_\lambda/F_{H\alpha}$	$(F_\lambda/F_{H\alpha})_{corr}$
Lα	1216	2.10	2.40	1.95	2.20	0.86	0.86
Hα	6563	1.00	1.00	1.00	1.00	1.00	1.00
Hβ	4861	...	...	0.37	0.37	0.25	0.25
$F_{H\alpha}(10^{-13}$ ergs $cm^{-2}s^{-1})$	...	0.64	0.65	2.00	2.04	11.1	11.1

[a] The line strength for Lα is taken from Osmer and Smith 1977. The determination of $E(B-V)$ for this object is based solely on the H I column density in the line of sight.

[b] The Hβ line flux is that determined by Soifer *et al.* (1979) normalized to our data such that the continuum levels are in agreement. The value of $E(B-V)$ for this object is suspect since the H I column density in the line of sight is poorly determined.

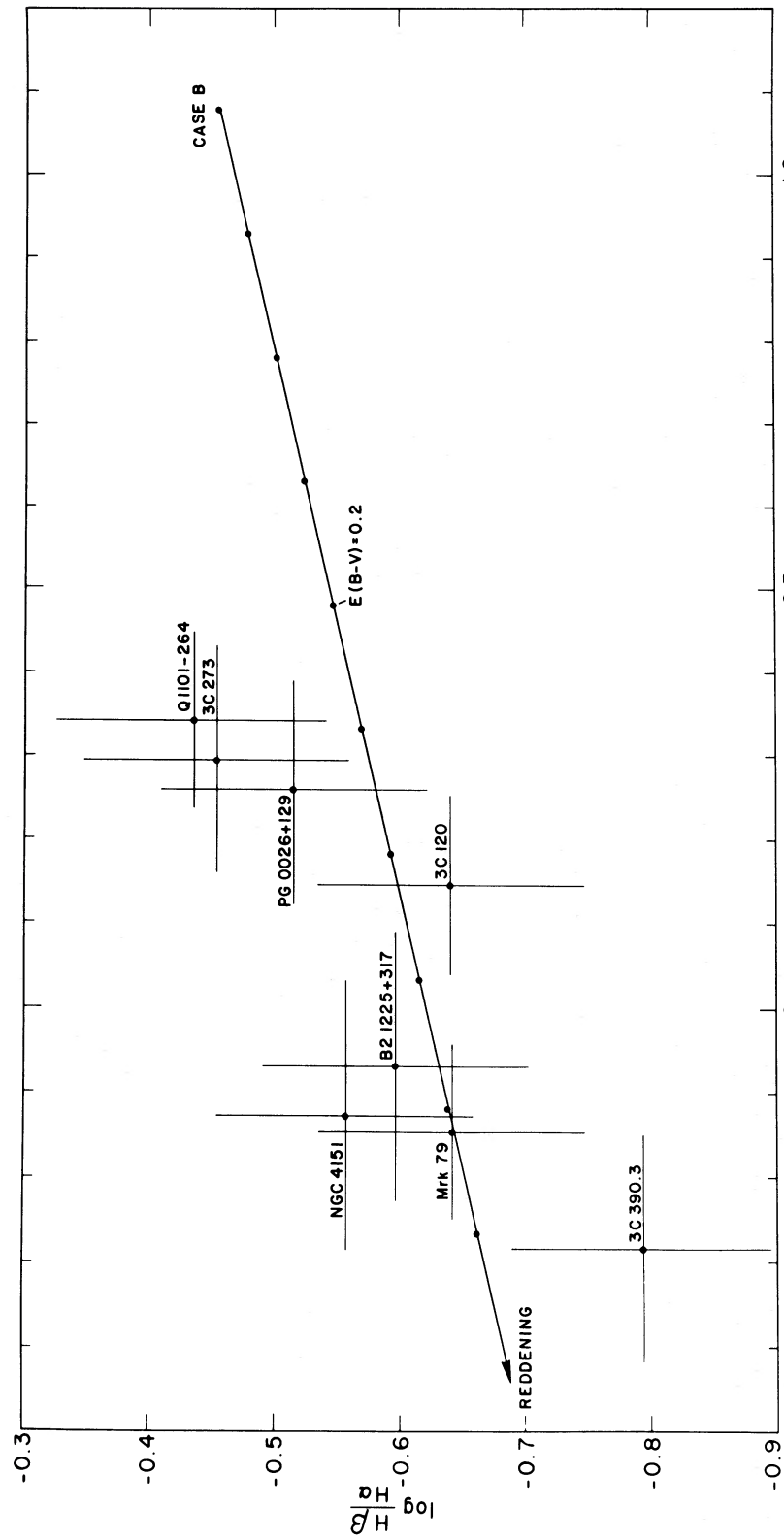

FIG. 2.—$H\beta/H\alpha$ versus $L\alpha/H\alpha$ for the three high-redshift QSOs and other broad line objects in our sample plus other broad line objects with published $L\alpha/H\alpha/H\beta$ ratios. The track that case B line ratios would take for different amounts of external reddening is plotted for comparison. Each tick mark on the case B track corresponds to an increase of 0.05 in $E(B-V)$. References for the published data are: NGC 4151, Davidsen (1980); Mrk 79, Oke and Lauer (1979), and Oke and Zimmerman (1979); B2 1225+317, Soifer *et al.* (1979) and Puetter *et al.* (1979); 3C 390.3, Ferland *et al.* (1979); Q1101−264, Osmer and Smith (1977); 3C 120, Oke and Zimmerman (1979); 3C 273, Boggess *et al.* (1979); PG 0026+129; Puetter *et al.* (1978) and Baldwin *et al.* (1978).

Osterbrock 1974). Also plotted in Figure 2 is the curve representing the locus of line ratios for case B combined with varying amounts of reddening due to galactic-type dust external to the line emitting region. Although the best-fit relation to these data would be somewhat steeper than the reddening curve, the results are consistent with intrinsic case B line ratios reddened by an amount corresponding to $E(B-V)\sim 0.2-0.4$. Based on results for other line ratios, we will argue that dust alone cannot produce the observed hydrogen line spectrum and that effects other than dust are likely to dominate. In the case of 3C 390.3, the dust, if present, must lie just outside the broad line region since the narrow components of the hydrogen lines suggest little or no reddening (Ferland *et al.* 1979). Nevertheless, since we know of no other process which naturally predicts the observed correlation, we suggest that dust may be present in these objects and might be important in determining the Lyman/Balmer line ratios.

The relation between the $L\alpha/H\alpha$ ratio and the UV-optical spectral index is plotted in Figure 3. In this case the spectral index, α, has been determined by assuming a uniform power law, $F_\nu \propto \nu^{-\alpha}$, in the continuum between $L\alpha$ and $H\alpha$. Again, reddening is a possible explanation for the observed correlation. Note, however, that for reddening to be the sole explanation of the $L\alpha/H\alpha$ ratio, the intrinsic continuum spectra must be quite flat or even rising into the UV as suggested by Netzer and Davidson (1979). Our limited understanding of the QSO continuum emission mechanism cannot preclude such models. However, the observation that some objects (e.g., 3C 373, Swanenburg *et al.* 1978) show a continuous spectrum with relatively constant spectral index, $\alpha\approx 1$, from radio to X-ray wavelengths suggests to us that this is not a general phenomenon.

The Paschen/Balmer line ratios should also be a sensitive indicator of the presence of dust. In Figure 4 we plot the $P\alpha/H\alpha$ ratio versus the Balmer decrement for our sample of low-redshift QSOs. For comparison we also plot the reddening track for case B line ratios. In this case several objects have line ratios that are inconsistent with case B plus reddening. In fact, the data appear to be correlated in a sense opposite to that expected from reddening.

Line ratios are not the only evidence that the intrinsic QSO emission line spectrum is not described by case B recombination. In Figure 5 we plot the rest frame equivalent width of $H\alpha$, $W_\lambda(H\alpha)$, versus the optical spectral index. The optical spectral index was determined by a least squares fit to selected optical continuum points after correction for galactic reddening. Several objects show a change of slope in the blue region of the spectrum which we interpret as due at least in part to Balmer continuum emission (see § III*b*). For these objects we used only the continuum points from the red portion of the spectrum. In all cases, except 4C 31.63 which is not plotted, the fit to a power law was quite good. For optically thin recombination models, assuming that all UV photons are absorbed, we may write

$$W_\lambda(H\alpha)=\varepsilon_A \frac{6563}{\alpha}\frac{\alpha_{H\alpha}}{\alpha_B}\left(\frac{6563}{912}\right)^{-\alpha} \qquad (1)$$

where ε_A is the covering factor, $\alpha_{H\alpha}$ is the effective recombination coefficient for $H\alpha$, α_B is the total case B recombination coefficient, and α is the intrinsic UV continuum spectral index. Assuming that the optical spectral index which we derive applies well below the Lyman limit, we have plotted the expected relation between $W_\lambda(H\alpha)$ and the observed optical spectral

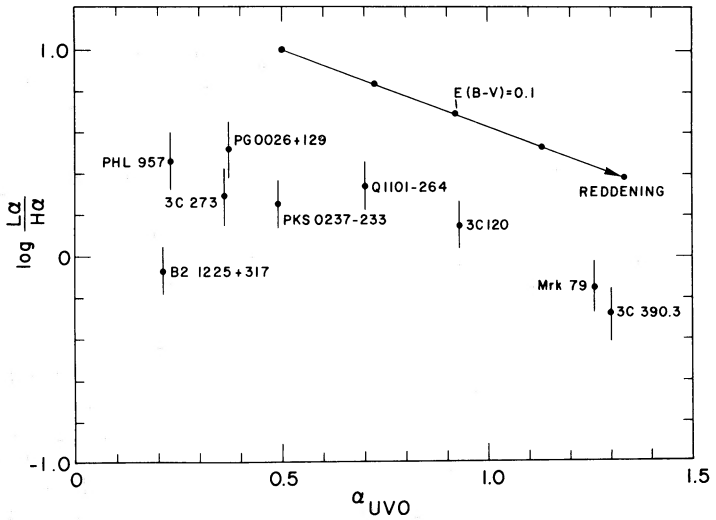

FIG. 3.—$L\alpha/H\alpha$ versus the spectral index as calculated from the continuum flux at 1216 Å and 6563 Å for the three high-redshift objects of our sample and other broad line objects with published $L\alpha/H\alpha$. The direction in which reddening takes the $L\alpha/H\alpha$ ratio is plotted for comparison. Note that the origin of the reddening curve has been arbitrarily positioned and that each tick mark along the curve corresponds to an increase in $E(B-V)$ of 0.05.

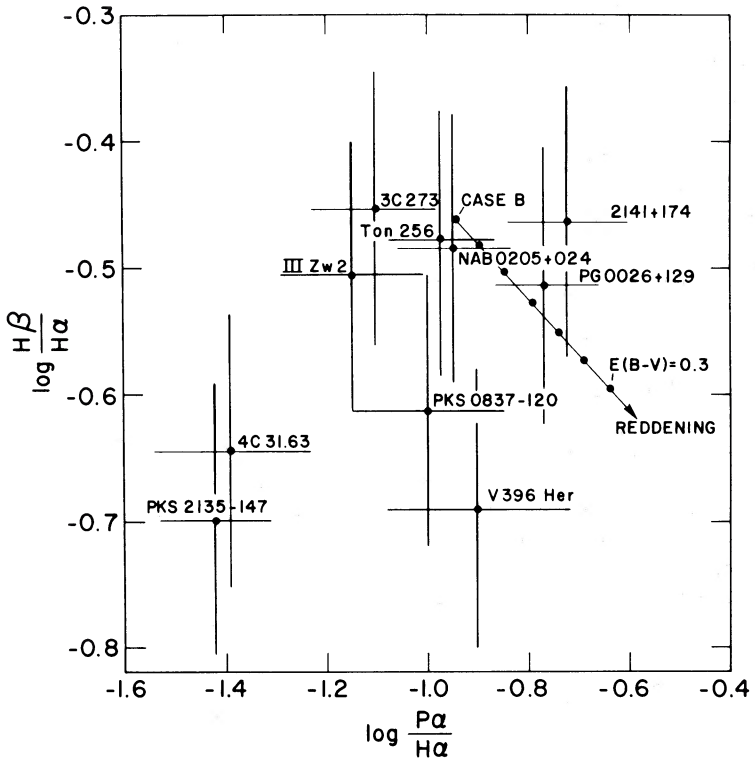

FIG. 4.—$H\beta/H\alpha$ versus $P\alpha/H\alpha$ for the low-redshift QSOs of our sample. The track that case B line ratios would take for different amounts of external reddening is plotted for comparison. Each tick mark along the reddening track corresponds to an increase of 0.05 in $E(B-V)$.

index for unity covering factor in Figure 5. The effects of decreasing covering factor and reddening are indicated by arrows. Several objects in Figure 5 lie above the predicted relation—that is, they show a larger equivalent width of $H\alpha$ than would be predicted if every UV ($\lambda < 912$ Å) photon photoionizes a hydrogen atom which recombines producing case B ratios. In principle, reddening may account for this effect, but we expect that the effects of reddening would be offset by the covering factor being much less than unity. In addition, other considerations suggest that reddening is not important for some of the objects that lie above the predicted curve. For example, the $P\alpha/H\alpha$ ratio and Balmer decrement of Ton 256 indicate little or no reddening in that object, thus requiring a covering factor near unity. A simplistic interpretation of this result is that $H\alpha$ is enhanced *above* case B ratios rather than that $L\alpha$ is depressed.

Other possible interpretations of this result include the following: (1) The optical spectral index is not indicative of the spectrum at ionizing energies. If α decreases considerably in the UV, then arbitrarily large $H\alpha$ (and also $L\alpha$) equivalent widths could be produced. (2) For QSOs that are highly variable the average $W_\lambda(H\alpha)$ could be lower than that plotted in Figure 5 if we observed the object in its quiescent state. As previously discussed, only III Zw 2 and PKS 2135−147 are known to be highly variable, but both Ton 256 and PKS 0837−120 do exhibit variability on the order of a few tenths of a magnitude (Grandi and Tifft 1974). The error bar for PKS 2135−147 in Figure 5 shows the range in $W_\lambda(H\alpha)$ for that object between our observations and those of Baldwin (1975). (3) Photoionization from the central object is not the excitation source for the broad-line region. Baldwin *et al.* (1977) have considered high-energy particle excitation as a possible mechanism, but concluded that this is unlikely due to the absence of emission features from species produced in spallation reactions. Shock excitation is also a possibility, but shock models do not generally agree well with the observed spectrum.

It is curious that Figure 5 shows a correlation opposite to that which would be predicted by photoionization models, in the sense that the steeper spectrum objects appear to have larger equivalent widths of $H\alpha$ than the hard spectrum QSOs. From the point of view of the number of photons available to ionize hydrogen, one would expect larger $H\alpha$ equivalent widths from harder ionizing spectra. It is possible that the correlation between α and $W_\lambda(H\alpha)$ indicates some dynamical mechanism in which UV radiation pressure decreases the amount of broad line gas present in the

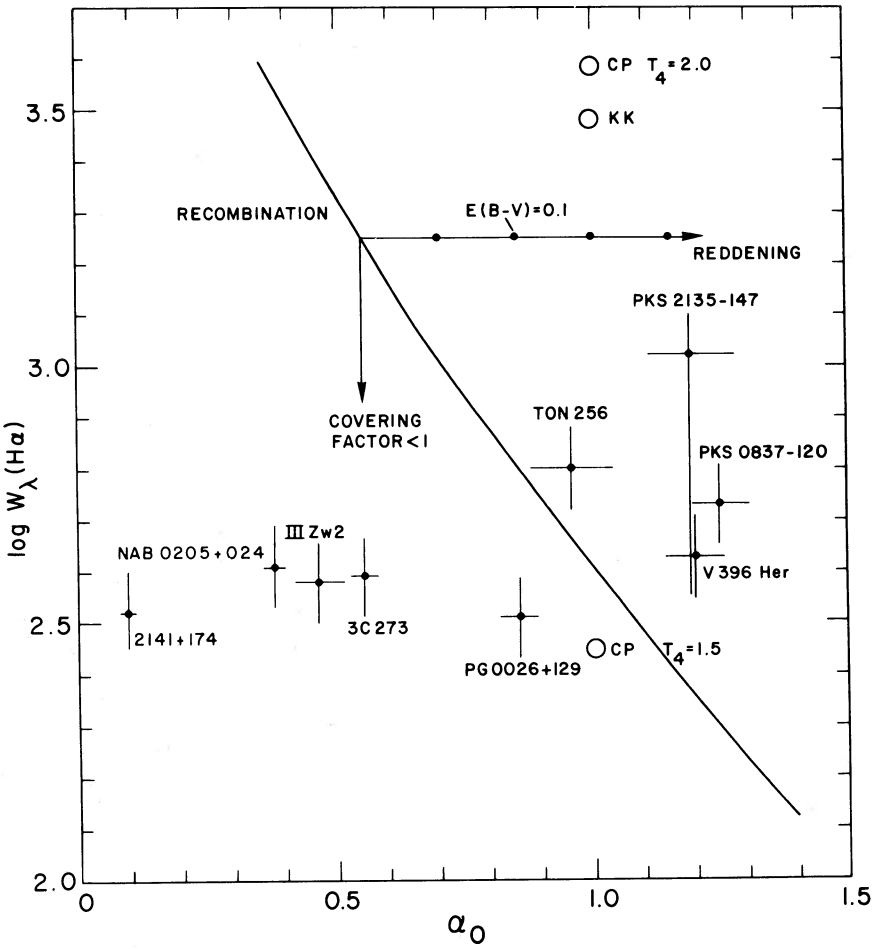

FIG. 5.—The rest frame equivalent width of Hα versus the optical spectral index for the low-redshift QSOs in our sample. The expected equivalent width for unity area covering factor for optically thin recombination assuming all UV photons are absorbed is plotted for comparison. The direction that the recombination curve would be displaced for reddening [each tick corresponding to 0.05 in $E(B-V)$] and covering factors less than unity are indicated by arrows. The equivalent widths assuming unity covering factor produced by the Kwan and Krolik (1979) model B and the $T_4 = 1.5$ and 2.0 models of Canfield and Puetter (1980, 1981*b*) are plotted as open circles. The error bars for PKS 2135−147 show the range of W_λ(Hα) due to continuum variability as well as the statistical error.

objects with flatter spectra. On the other hand, there is no clear correlation between W_λ(Hα) and the observed optical luminosity assuming cosmological distances, nor between line velocity width and spectral index or luminosity as might be expected if such a mechanism were operating.

Another question concerning dust reddening models is: In what region of the spectrum will the absorbed UV radiation be reradiated by the dust? For a power law spectrum with spectral luminosity $L_\nu = \kappa \nu^{-\alpha}$ and $\alpha = 1$ the ratio of the reradiated blackbody flux to the nonthermal flux at blackbody maximum will be

$$\frac{L^{\rm BB}_{\nu_{\rm max}}}{L^{\rm NT}_{\nu_{\rm max}}} = \frac{32\pi hc^2}{\sigma}\,\frac{L^{\rm UV}}{\kappa}\,\frac{1}{\exp(2\,hc/k)-1}, \qquad (2)$$

where $L^{\rm UV}$ is the absorbed nonthermal ultraviolet luminosity ($= L^{\rm BB}$ = total radiated thermal luminosity from dust). For most objects in our sample, the available infrared photometry is insufficient to rule out the presence of a strong thermal component due to dust. However, for 3C 273 there is relatively good photometry or upper limits (Hildebrand *et al.* 1977) from the near-IR to millimeter wavelengths. If the UV continuum of 3C 273 is uniformly depressed by the factor of 5 necessary to explain the Lα/Balmer ratios, we find

$$L^{\rm BB}_{\nu_{\rm max}} / L^{\rm NT}_{\nu_{\rm max}} = 6. \qquad (3)$$

Such a large departure from a power law in 3C 273 is ruled out in all well observed regions of the spectrum.

TABLE 5

OBSERVATIONAL AND THEORETICAL HYDROGEN LINE SPECTRA

RATIO	PG 0026+129	3C 273	STD QSO	CASE B	KWAN AND KROLIK MODEL B	CANFIELD AND PUETTER[a] $T_4=1.5$	CANFIELD AND PUETTER[a] $T_4=2.0$
$L\alpha/H\alpha$....	1.8	2.0	2.0	12	1.9	2.1	1.7
$H\beta/H\alpha$ ...	0.31	0.35	0.33	0.35	0.21	0.31	0.37
$H\gamma/H\alpha$ ...	0.10	0.15	0.14	0.16	...	...	...
$H\delta/H\alpha$ ...	0.04	0.04	0.05	0.09	...	...	...
$Bc/H\alpha$[b] ...	0.9	2.0	1.2	1.4	0.55	2.4	1.5
$P\alpha/H\alpha$....	0.17	0.08	0.12	0.12	0.12	0.10	0.09

[a] These models assume a constant hydrogen density of $n_H = 10^{10}$ cm^{-3} and an ionizing flux distribution $\mathcal{F}(\nu) \propto \nu^{-1.0}$ with $\mathcal{F}(\nu) = 10^{-8}$ ergs cm^{-2} s^{-1} at 1 Rydberg.

[b] Bc = Balmer continuum.

In the unobserved region between 10 μm and 100 μm a 150 K thermal source of the requisite luminosity could marginally exist within observed limits. An improved limit at 100 μm or a good limit at 20 μm would easily rule this out. Certainly some Seyfert galaxies (e.g., NGC 4151, NGC 1068 [Cutri *et al.* 1981]) show clear evidence for thermal dust emission, but there is no evidence for significant amounts of dust in 3C 273. As we will see, this is consistent with the interpretation of 3C 273's spectrum as representative of the "intrinsic" unreddened QSO spectrum, whereas NGC 4151 can be seen to be further along the reddening curve in Figure 2.

The data were searched for a number of other correlations between line intensity, line width, luminosity, spectral index, etc. In none of these cases was a significant correlation found.

One of the goals of this program has been to obtain the "intrinsic" hydrogen emission spectrum of the broad line region for comparison with theoretical models. In Table 5 we have attempted to synthesize the spectrum of a "standard" QSO from our data. The clumping of objects near $L\alpha/H\alpha \approx 2$ in Figure 2 and the lack of objects with $L\alpha/H\alpha \gtrsim 2$ suggests that this may be a reasonable estimate of the intrinsic $L\alpha/H\alpha$ ratio. From Tables 3 and 4 we can see that among objects for which we have reasonably complete observations, there are five QSOs which have very similar line ratios. These are PG 0026+129, NAB 0205+024, 3C 273, Ton 256, and 2141+174. For the standard QSO Balmer and Paschen line ratios we have used an average of the ratios for these objects. Note, however, that there is a large variation in the $P\alpha/H\alpha$ ratio among the low-redshift objects. Thus the value we quote for this ratio in the standard QSO must be considered poorly determined. There are two QSOs, PG 0026+129 and 3C 273, for which lines from all three series have been observed. The line ratios for these two QSOs are also listed in Table 5 along with the integrated Balmer continuum emission ratioed to $H\alpha$. The identification of the Balmer continuum emission is discussed below. One can see that the line ratios in these two objects are very similar to those of the standard QSO. For want of a better choice, we will adopt the line ratios shown in Table 5 for the purpose of further discussion.

One can see, both from our standard spectrum and also from the spectra of individual objects, that case B ratios with dust reddening alone cannot explain the hydrogen line ratios. The $P\alpha/H\alpha$ ratios suggest little or no reddening and, in some cases, lie significantly below the case B ratio, whereas reddening would increase the ratio. On the other hand, the $L\alpha/H\alpha$ ratio and Balmer decrement would suggest moderate reddening. The intensities of the higher Balmer series members are not well determined, but there does appear to be a uniform tendency for the Balmer decrement to steepen with increasing series member relative to case B values. These results confirm those of Puetter *et al.* (1978), who suggested that the reddening curves required to produce the spectra of PG 0026+129 and 3C 273 are not physically reasonable.

As discussed previously, there have been a number of recent attempts at modeling QSO broad line spectra which include more realistic treatments of radiative transfer effects. One of the most detailed recent calculations is that of Kwan and Krolik (1979), who have calculated a self-consistent thermal structure for emission line clouds including the effects of heavy elements. Their models are able to produce many of the observed features of QSO broad line spectra, including the low $L\alpha$/Balmer line ratio. In these models, collisional ionization and photoionization from the higher bound levels by the nonthermal continuum allow the clouds to remain relatively highly ionized ($n_e/n_H \approx 0.3$) to very large optical depths ($\tau_{L\alpha} \gtrsim 10^8$). This results in enhanced Balmer emission from this extended region

where Hα is the dominant coolant. Comparison of Kwan and Krolik's model B with our standard ratios shows relatively good agreement: considerably improved over case B ratios. Their model, however, produces a steeper Balmer decrement than is observed and fails to produce sufficient emission in the Balmer continuum (Bc).

Another recent calculation by Canfield and Puetter (1980, 1981*a*, *b*) presents a more detailed calculation of the radiative transfer, at the expense of assuming that the emission line clouds are isothermal and composed purely of hydrogen. The principal improvement in these calculations is the treatment of the photon escape probability in the wings of the nonresonance lines, resulting in considerably higher escape probabilities than used by Kwan and Krolik (a factor of 25 in Hα, for example). Their predicted line intensity ratios are qualitatively similar to those of Kwan and Krolik. They also find an extended, ionized zone which principally produces Balmer emission. In this case the ionization is near unity due to upper level ionization from the higher bound-free *diffuse* continua. Line ratios for two Canfield and Puetter models, $T_4 = 1.5$ and $T_4 = 2.0$, are also presented in Table 5. They are in relatively good agreement with our standard QSO spectrum with the possible exception that they produce too much Balmer continuum. This, however, is probably the most poorly determined ratio observationally, owing to the sensitivity to selection of continuum interval and shape. It is not clear that poor agreement with the Bc/Hα ratio should be considered a significant weakness for either class of models.

Because Hα emission is enhanced in both the models of Kwan and Krolik and those of Canfield and Puetter, they are capable of producing the observed Hα equivalent widths. The points appropriate to the models listed in Table 5 for unity covering factor have been plotted in Figure 5 for comparison with the observations. The models of Kwan and Krolik produce considerable Hα emission: for reasonable values of the covering factor, $\varepsilon_A \lesssim 0.1$, the isothermal models require high temperatures $T_e \approx 2 \times 10^4$ K. The requirement of such a large temperature in the Balmer line producing region will be a sensitive test of these models when thermal balance is fully included.

b) *Balmer Continuum*

The presence of a broad feature between roughly 4000 Å and 2000 Å in the spectra of QSOs has been recognized by a large number of authors (Baldwin 1975; Neugebauer *et al.* 1979; Richstone and Schmidt 1980), and a wide range of identifications have been suggested (see Richstone and Schmidt 1980). These identifications include emission from a 12,000 K thermal source, synchrotron emission from monoenergetic particles, starlight from a superposed galaxy, the presence of a large number of unresolved emission lines, and Balmer continuum emission.

Most of the above explanations have difficulties (Richstone and Schmidt 1980). The thermal emission mechanism has a spectral peak which is extremely temperature sensitive and produces a feature which is somewhat too broad. The synchrotron mechanism produces a feature much too broad to be plausible as well as being very sensitive to the magnetic field strength and particle energy distribution. The starlight interpretation seems unlikely since normal spirals and elliptical galaxies have insufficient flux below 3800 Å to account for the observed feature, unless the QSO "event" has triggered the formation of stars in the recent past as suggested by van den Bergh (1975). In addition, the flux distribution due to stars would also be too broad to explain this feature. The basic difficulty with the Balmer continuum interpretation has been considered to be the relative strength of the integrated Balmer continuum emission (Bc) compared to the Hβ line flux, and the shape of the continuum feature. Following Baldwin (1975), we attribute the bulk of this feature to Balmer continuum emission. We attribute the remainder of this feature to superposed line emission, principally from multiplets of Fe II. In Figure 6 we show this part of the spectrum of 4C 31.63 shifted back to the QSO rest frame. Plotted on the spectrum is the optically thin Balmer continuum spontaneous recombination spectrum given by

$$F(\nu) = F(\nu_0)\exp[-h(\nu-\nu_0)/kT]; \quad \nu \gtrsim \nu_0 \qquad (4)$$

(see, for example, Jefferies 1968) and adopting $T = 10^4$K. Apart from the bumpy structure superposed on top, the general continuum structure agrees relatively well with the continuum shape. The extension longward of 3646 Å is undoubtedly due to the velocity broadening of the continuum itself and to the convergence of the higher members of the Balmer series. For the velocity width of 3300 km s^{-1} determined for 4C 31.63 the half maxima of the Balmer lines overlap for H8 and H9 (3889, 3835 Å). Also shown on Figure 6 is the multiplet structure of Fe II in this spectral region. As will be discussed in § III*c*, we attribute the "excess" emission at the Balmer continuum to be due to blended emission lines, principally those of Fe II. Assuming that this bump is due to Balmer continuum emission, we have used the height of the bump above the nonthermal continuum at 3646 Å to estimate the integrated strength of the Balmer continuum by:

$$F_{\rm Bc} = \frac{F(\nu_0)kT}{h}, \qquad (5)$$

using a temperature which best fits the Balmer continuum shape in that region. Because of the complicated nature of the continuum in this region, the necessity of extrapolating the underlying nonthermal continuum, and the sensitivity to T, the values of $F_{\rm Bc}$

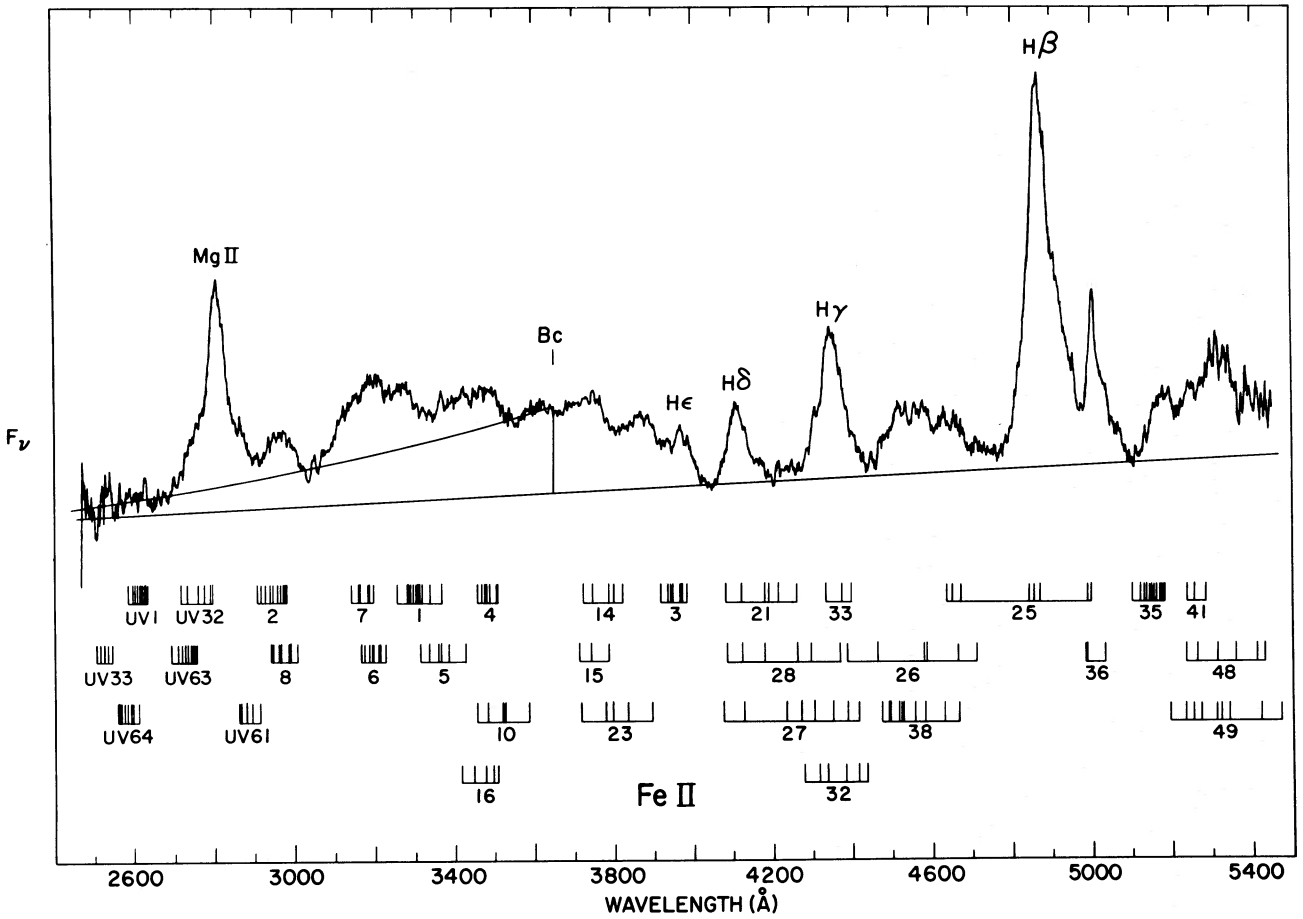

FIG. 6.—The spectrum of 4C 31.63 (rest frame) in the region of the Balmer continuum edge at 10 Å resolution. Plotted for comparison are the positions of a number of Fe II multiplets and the expected Balmer continuum flux for optically thin Balmer continuum emission from 10,000 K gas.

are not particularly well determined. Although choosing a temperature for the Balmer continuum is somewhat qualitative in nature, temperatures in the range 7500–10,000 K produce an adequate fit to the observed spectra, but temperatures as high as 15,000 K produce too much flux at $\lambda \lesssim 2600$ Å. The Balmer continuum/line ratios found in this study are in relatively good agreement with recent theoretical models in which the Balmer lines are optically thick, but the continuum is optically thin with $T_e \approx 7000$–$10{,}000$ K. If the temperatures we derive are correct, the Balmer continuum emission must come from somewhat higher optical depth than the region producing the lines, since covering factor arguments suggest that $T_e \gtrsim 15{,}000$ K in the line-forming region. This result is consistent with the model calculations discussed here since both the Kwan and Krolik and the Canfield and Puetter models produce the Balmer continuum emission from regions deeper into the cloud where T_e will be smaller. In order for the Balmer continuum emission to be optically thin, the column density of hydrogen in level 2 must be $\lesssim 2 \times 10^{17}$ cm^{-2}, which for the Canfield and Puetter models implies $\tau_{L\alpha} \lesssim 3 \times 10^6$ in the emitting clouds.

Recently, Grandi and Phillips (1980) have suggested that there are several problems with this identification. They argue that there is no correlation between the observed strength of the "bump" and the Hβ flux, as might be expected. For optically thick models such as those of Canfield and Puetter, no strong Hβ/Bc correlation is expected because the ratio will depend sensitively on the optical depth in the Balmer continuum. Grandi and Phillips also note that in some cases the excess emission shortward of λ3646 rest does not decline as would the Balmer continuum. We do not suggest that the Balmer continuum accounts for all of the emission shortward of λ3646, only part of it, or that this "bump" must have the same origin in all QSOs. Our sample of objects does appear to be well fitted by a combination of Balmer continuum and Fe II emission.

c) Fe II *Lines*

The presence of Fe II lines in Seyfert 1 galaxies and in some QSOs is well established. Strong optical Fe II emission in the 3000–7000 Å region has been observed in a number of objects (Phillips 1979*a*; Osterbrock 1977). Fe II UV transitions also have been identified in a number of QSOs (Wills *et al.* 1979). The spectra of the low-redshift QSOs in our sample show a number of broad bumps, particularly near the Balmer continuum and near the Mg II λ2800 emission line. In addition, the λ2950 feature seen in many QSOs is also present.

Figure 6 shows an enlarged view of the blue portion of the spectrum of 4C 31.63. This object is one of the objects in our sample showing strong Fe II emission. The positions of a number of Fe II transitions have been plotted for comparison with the data. As can be seen from the figure, a great deal of the unusual shape of the Balmer continuum region can be attributed to strong Fe II emission. The large bump at ~3200 Å is probably predominantly due to multiplets 6 and 7, although there may be some contribution from He I λ3188 and He II λ3203. The bump at 3250 Å is probably due to multiplet 1, and the emission between 3350 Å and 3550 Å is probably dominated by multiplets 4, 5, and 16 with perhaps a small contribution from multiplet 10.

The feature near 2950 Å in Figure 6 has been observed in a large number of objects (Phillips 1978*a*; Grandi and Phillips 1978, 1979). This feature has been attributed in the past to a variety of transitions. Past identifications include [Mg V] λ2931 (Lynds and Wills 1968), Mg II λ2934 (Grandi and Phillips 1978), and various blends of [Ne V] λ2974 and [O I] λ2972. The forbidden line identifications seem unlikely since the observed feature has the typical broad character of a permitted transition. The Mg II λ2934 identification agrees poorly in wavelength with the observed emission, at least in 4C 31.63. Following the suggestion of Wills *et al.* (1979), we attribute this feature to Fe II multiplets 2 and 8. The strong evidence of other Fe II emission in these objects seem to make the Fe II identification of the λ2950 feature quite natural.

In many broad line objects the Mg II λ2800 emission is observed to be considerably broader than the Balmer lines (Grandi and Phillips 1979) or appears to sit on the top of a broad hump. We suggest that this is due to the presence of significant Fe II emission at wavelengths close to the Mg II peak. Wills *et al.* (1979) identify the narrow λ2750 feature in PKS 2216−03 as due to multiplets UV62 and UV63. These lines probably also significantly broaden the apparent Mg II λ2800 emission in a number of QSOs. Figure 6 shows that this is certainly a plausible explanation of the large blue wing of Mg II λ2800 seen in 4C 31.63. In addition, we feel that the red wing of λ2800 is also broadened by Fe II emission, possibly by UV61 and other multiplets. As can be seen from the figure, uncertainty in the amount of Fe II emission due to low resolution data or poor signal-to-noise can lead to errors as large as a factor of 2 in the Mg II line strength.

Theoretical interpretations of the Fe II emission have been discussed by a large number of authors (Wampler and Oke 1967; Bahcall and Kozlovsky 1969; Adams 1975; Oke and Shields 1976; Osterbrock 1977; Boksenberg and Netzer 1977; Phillips 1978*b*; Collin-Souffrin *et al.* 1979; Netzer 1980; Grandi and Phillips 1980). Among the proposed excitation mechanisms for the Fe emission are ultraviolet fluorescence of the optical lines and direct collisional excitation. In support of the fluorescence interpretation, there is sufficient total energy in the continuum at the wavelengths of the UV transitions to produce the observed optical lines. However, recent work by Wills *et al.* (1979) indicate that the UV transitions are in emission rather than in absorption as might be expected in this model. It is interesting to note that the UV resonance lines are not considerably stronger than the optical features arising from the same upper level. For example, we do not see any significant emission at λ2599 (UV1) in 4C 31.63, but there is emission near Hα which we attribute to multiplet 40. The branching ratio, however, favors λ2599 by 10^4:1 (Phillips 1979*c*). The low observed UV1/multiplet 40 ratio can be interpreted as due to radiative transfer effects as is discussed below.

Two recent detailed studies of the radiative transfer in Fe II lines are those of Collin-Souffrin *et al.* (1979) and Netzer (1980). These works separate out a set of lines that interact strongly with each other and interact only very weakly with other Fe II lines. The work of Netzer includes more physical processes and a slightly greater number of transitions than do Collin-Souffrin *et al.* The results of this calculation appear to depend strongly on the particular model, and only a limited range of parameter space is explored. Furthermore, Collin-Souffrin *et al.* solve the full frequency-dependent and depth-dependent radiative transfer equation rather than using escape probabilities or mean number of scatterings. In addition, they explore a much wider range of parameter space. For these reasons we choose to discuss our results in terms of the calculations of Collin-Souffrin *et al.*

Collin-Souffrin *et al.* conclude that in order to produce optical Fe II emission that is comparable or greater than the UV emission, large optical depths in the UV transitions are required ($\tau_{UV3} \sim 10^2$ for $T_e = 10^4$ K and $\tau_{UV3} \sim 10^3$ if $T_e = 2 \times 10^4$ K). In their models the excitation may be due to resonance fluorescence for $T_e = 10^4$ K while it is certainly collisional if $T_e = 2 \times 10^4$ K. These conclusions were based on an assumed ionized fraction, $n_e/n_H = 0.004$ for $T_e = 10^4$ K, and $n_e/n_H \approx 1.0$

for $T_e = 2 \times 10^4$ K. Recent theoretical studies suggest, however, that the ionized fraction will be unity until the electrons cool below $T_e \approx 7 \times 10^3$ K (Canfield and Puetter 1980, 1981*b*). In this case, the results of Collin-Souffrin *et al.* indicate that the excitation mechanism is almost certainly collisional for $T_e \gtrsim 7 \times 10^3$ K.

While large optical depths in the Fe II lines might at first seem surprising, they are to be expected if the hydrogen lines are very optically thick. The relationship between $\tau_{L\alpha}$ and τ_{UV3} is

$$\frac{\tau_{UV3}}{\tau_{L\alpha}} = \left(\frac{\sigma_{UV3}}{\sigma_{L\alpha}}\right)\left[\frac{n(\text{Fe})}{n(\text{H})}\right]\frac{n(\text{Fe II})/n(\text{Fe})}{n(\text{H}^0)/n(\text{H})}. \quad (6)$$

If in a given cloud the line width is purely due to thermal velocities and the iron abundance is solar, we obtain

$$\frac{\tau_{UV3}}{\tau_{L\alpha}} \approx 10^{-4}\frac{n(\text{Fe II})/n(\text{Fe})}{n(\text{H}^0)/n(\text{H})}. \quad (7)$$

Finally, if we take values of $\tau_{L\alpha} \approx 10^6$ and $n(\text{H}^0)/n(\text{H}) \approx 10^{-3}$ (corresponding to Canfield and Puetter 1980, 1981*b* models with $T_e \approx 1.5$–2.0×10^4 K, which produce the observed hydrogen line ratios), we obtain

$$\tau_{UV3} \sim 10^5 \frac{n(\text{Fe II})}{n(\text{Fe})}. \quad (8)$$

The ratio of $n(\text{Fe II})/n(\text{Fe})$ is very difficult to determine. For example, the value that Collin-Souffrin *et al.* obtain for $n(\text{Fe II})/n(\text{Fe})$ is based on an assumed ionized fraction of hydrogen and questionable values of available ionizing flux. In their calculation the majority of Fe is in the form of Fe III if there is significant radiation at the Fe II ionization edge. At the depths Fe II emission is likely to form, the Lyman continuum is very thick ($\tau \approx 10^2$–10^3). The radiation available to ionize Fe II to Fe III at these optical depths will thus be diffuse Lyman continuum radiation. Therefore, the ionization structure of Fe is intimately related to the radiative transfer in hydrogen. Nonetheless, in view of equation (8) we feel it is likely that $\tau_{UV3} \gtrsim 10^2$ unless iron is very underabundant.

Finally, since Fe II lines are probably quite thick, it seems reasonable that other metal lines are also quite thick. Equation (6) along with optical depths in Lα of 10^6 and $n(\text{H}^0)/n(\text{H}) \approx 10^{-3}$ seems to guarantee that all the resonance lines of the abundant ions are thick.

IV. SUMMARY

We have presented a variety of evidence indicating that QSO broad line emitting clouds have very large optical depths both in the lines of hydrogen (Lyman and Balmer; $\tau_{L\alpha} \approx 10^6$) and in the resonance lines of the abundant heavy elements. Our best estimate of the "intrinsic" hydrogen spectrum is inconsistent with simple optically thin recombination reddened by dust, but is in qualitative agreement with recent optically thick radiative transfer calculations with temperature $T_e \gtrsim 1.5 \times 10^4$ K in the line emitting region.

We attribute much of the structure seen in the "continuum" to Balmer continuum emission plus blends of broad permitted lines, principally those of Fe II. Our results for the Balmer continuum are consistent with optically thin emission in this transition from a region with $T_e \lesssim 10^4$ K, which is significantly cooler than the line emitting region.

The data presented show evidence of small amounts of dust [$E(B-V) \lesssim 0.2$], but suggest that dust reddening does not dominate the broad line ratios. The lack of correlations among observed properties such as line strengths, widths, continuum luminosity, etc., and the presence of some "anomalous" correlations (e.g., W_λ versus α_0) indicate that factors other than those considered in present models are probably important in the physics of the broad line emitting region. Full dynamical models incorporating radiative transfer effects will probably be necessary to treat the broad line region completely.

Several additional observations would further our understanding of the broad line region. Observations of the He lines, especially He I λ10830 with respect to other helium triplet features, would allow us to probe the optical depth in helium. Further combined UV-optical-IR studies which would allow the measurement of line strengths in the Lyman, Balmer, and Paschen series in individual objects will hopefully allow us to produce specific models rather than general composite models. Finally, it would be of interest to see even more detailed theoretical treatments of the optically thick clouds, along the lines already begun by several authors. Of particular importance are thermal balance calculations which treat photon escape and heating in all energetically important transitions in a physically meaningful way. This would result in an emission cloud temperature profile which could be used in radiative transfer calculations aimed at deducing elemental abundances, area covering factors, etc.

We wish to acknowledge the contribution of B. T. Soifer who participated in the early phases of this program and who has freely discussed his own results with us, and also R. C. Canfield who provided useful discussions and suggestions. R.C.P. and H.E.S. acknowledge participation in the 1978 Santa Cruz Summer Workshop on Quasars and Active Galactic Nuclei, where this topic was actively discussed. We are grateful to R. Cutri, G. Jung, and V. Junkkarinen for assistance

with the observations and data reduction and to E. O. Smith for preparation of figures. Special thanks go to the staffs of Lick Observatory, KPNO, and CTIO, particularly J. Elias and R. Joyce, for their assistance. Extragalactic optical and infrared astronomy at UCSD is supported by the National Science Foundation under grants AST 77-22560, AST 76-82890, and AST 79-16885.

APPENDIX

The standards used for this program have been calibrated directly from observations of Vega over a period of almost 3 years. The internal consistency of the magnitudes as tested by measurements on nights of optimal conditions leads us to believe the absolute magnitudes listed in Table 6 are accurate to about 2% except as otherwise noted. The magnitudes listed are consistent with the calibration of Vega by Oke and Schild (1970) and the fluxes for zero magnitude given by Neugebauer *et al.* (1979).

TABLE 6

STANDARD STARS

Star	α(1950)	δ(1950)	Spectral Type	m_v	[1.25]	[1.65]	[2.28]	[3.5]
72 Psc ...	$1^h\ 2^m 26^s$	14°40′42″	F2	5.7	4.88	4.60	4.55	4.50
π^4 Ori ...	4 48 32	5 31 17	B3	3.8	4.12	4.09	4.14	4.15
λ Gem ...	7 14 13	16 37 55	A2	3.6	3.40[a]	3.33	3.30	3.28
54 Leo ...	10 52 54	25 1 1	A0	4.5	4.45	4.36	4.31	
ϵ Her	16 58 22	30 59 55	A0	4.3		3.87	3.85	3.90
ν Cyg[a] ...	20 55 18	40 58 24	A0	3.9	3.77	3.67	3.65	3.73

[a] The magnitudes marked are less certain than the rest. They are, however, probably accurate to 5%.

REFERENCES

Adams, T. F. 1975, *Ap. J.*, **196**, 675.
Bahcall, J. A., and Kozlovsky, B. Z. 1969, *Ap. J.*, **155**, 1077.
Baldwin, J. A. 1975, *Ap. J.*, **201**, 26.
_____. 1977, *M.N.R.A.S.*, **178**, 67P.
Baldwin, J. A., Boksenberg, A., Burbidge, G., Carswell, R., Cowsik, R., Perry, J., and Wolfe, A. 1977, *Astr. Ap.*, **61**, 165.
Baldwin, J. A., and Netzer, H. 1978, *Ap. J.*, **226**, 1.
Baldwin, J. A., Rees, M. J., Longair, M. S., and Perryman, M. A. C. 1978, *Ap. J. (Letters)*, **226**, L57.
Boggess, A., *et al.* 1979, *Ap. J. (Letters)*, **230**, L131.
Boksenberg, A., and Netzer, H. 1977, *Ap. J.*, **212**, 37.
Boksenberg, A., Shortridge, K., Fosbury, R., Penston, M. and Savage, A. 1975, *M.N.R.A.S.*, **172**, 289.
Burstein, D., and Heiles, C. 1978, *Ap. J.*, **225**, 40.
Canfield, R. C., and Puetter, R. C. 1980*a*, *Ap. J. (Letters)*, **236**, L7.
_____. 1981*a*, *Ap. J.*, **243**, 381.
_____. 1981*b*, *Ap. J.*, **243**, 390.
Collin-Souffrin, S., Joly, M., Reidmann, N., and Dumont, S. 1979, *Astr. Ap.*, **72**, 293.
Cutri, R. M., Jones, B., Merrill, K. M., Puetter, R. C., Russell, R. W., Soifer, B. T., and Willner, S. P. 1981, *Ap. J.*, submitted.
Davidsen, A. 1980, in *IAU Symposium 92, Objects of High Redshift*, ed. G. Abell and P. J. E. Peebles (Dordrecht: Reidel), p. 235.
Davidsen, A., Hartig, G., and Fastie, W. 1977, *Nature*, **269**, 203.
Ferland, G., and Netzer, H. 1979, *Ap. J.*, **229**, 274.
Ferland, G. J., Rees, M. J., Longair, M. A., and Perryman, M. A. C. 1979, *M.N.R.A.S.*, **187**, 65p.
Grandi, S. A., and Phillips, M. M. 1978, *Ap. J.*, **220**, 426.
_____. 1979, *Ap. J.*, **232**, 659.
_____. 1980, *Ap. J.*, **239**, 475.
Grandi, S. A., and Tifft, W. G. 1974, *Pub. A.S.P.*, **86**, 873.
Grasdalen, G. L. 1976, *Ap. J. (Letters)*, **208**, L11.
Green, R. 1976, *Pub. A.S.P.*, **88**, 665.
Greenstein, J. L. 1968, *Ap. J.*, **152**, 431.
Hildebrand, R. H., Whitcomb, S. E., Winston, R., Stiening, R. F., Harper, D. A., and Moseley, S. H. 1977, *Ap. J.*, **216**, 698.
Hyland, A., Becklin, E. E., and Neugebauer, G. 1978, *Ap. J. (Letters)*, **220**, L73.
Jefferies, J. T. 1968, *Spectral Line Formation*, (Waltham: Blaisdell).
Krolik, J., and McKee, C. 1978, *Ap. J. Suppl.*, **37**, 459.
Kwan, J., and Krolik, J. H. 1979, *Ap. J. (Letters)*, **223**, L91.
London, R. 1979, *Ap. J.*, **228**, 8.
Lowrance, J. L., Morton, D., Zucchino, P., Oke, J., and Schmidt, M. 1972, *Ap. J.*, **171**, 233.
Lynds, R., and Wills, D. 1968, *Ap. J. (Letters)*, **153**, L23.
Mathews, W. G., Blumenthal, G. R., and Grandi, S. A. 1980, *Ap. J.*, **235**, 971.
Netzer, H. 1975, *M.N.R.A.S.*, **171**, 395.
_____. 1980, *Ap. J.*, **236**, 406.
Netzer, H., and Davidson, K. 1979, *M.N.R.A.S.*, **187**, 871.
Neugebauer, G., Oke, J. B., Becklin, E. E., and Matthews, K. 1979, *Ap. J.*, **230**, 79.
Oke, J. B., and Lauer, T. R. 1979, *Ap. J.*, **230**, 360.
Oke, J. B., and Schild, R. 1970, *Ap. J.*, **161**, 1015.
Oke, J. B., and Shields, G. A. 1976, *Ap. J.*, **207**, 713.
Oke, J. B., and Zimmerman, B. 1979, *Ap. J. (Letters)*, **231**, L13.
Osmer, P. S., and Smith, M. G. 1977, *Ap. J.*, **213**, 607.
Osterbrock, D. E. 1974, *Astrophysics of Gaseous Nebulae* (San Francisco: Freeman).
_____. 1977, *Ap. J.*, **215**, 733.
Phillips, M. M. 1978*a*, *Ap. J. Suppl.*, **38**, 187.
_____. 1978*b*, *Ap. J.*, **226**, 736.
_____. 1979*c*, *Ap. J. Suppl.*, **39**, 377.

Puetter, R. C., Smith, H. E., Soifer, B. T., Willner, S. P., and Pipher, J. L. 1978, *Ap. J.* (*Letters*), **226**, L53.
Puetter, R. C., Smith, H. E., and Willner, S. P. 1979, *Ap. J.* (*Letters*), **227**, L5.
Richstone, D. O., and Schmidt, M. 1980, *Ap. J.*, **235**, 377.
Rieke, G., and Lebofsky, M. 1979, *Ap. J.*, **227**, 710.
Sargent, W. L. W. 1967, *Ap. J.* (*Letters*), **148**, L147.
Savage, B. D., and Mathis, S. M. 1979, *Ann. Rev. Astr. Ap.*, **17**, 73.
Shane, C. D., and Wirtanen, C. A. 1967, University of California Publications of the Lick Observatory, 22, part 1.
Shuder, J. M., and MacAlpine, G. M. 1979, *Ap. J.*, **230**, 348.
Smith, H. E. 1975, *Ap. J.*, **199**, 591.
_____. 1980, *Ap. J.* (*Letters*), **241**, L137.
Soifer, B. T., Oke, J. R., Matthews, K., and Neugebauer, G. 1979, *Ap. J.* (*Letters*), **227**, L1.
Swanenburg, B. N., *et al.* 1978, *Nature*, **275**, 298.
van den Bergh, S. 1975, *Ann. Rev. Astr. Ap.*, **13**, 217.
Wampler, E. J., and Oke, J. B. 1967, *Ap. J.*, **148**, 695.
Wills, B. J., Netzer, H., Uomoto, A. K., and Wills, D. 1979, preprint.

J. L. PIPHER: Physics and Astronomy Department, University of Rochester, Rochester, NY 14627

R. C. PUETTER, HARDING E. SMITH, and S. P. WILLNER: Center for Astrophysics and Space Sciences, C-011, University of California, San Diego, La Jolla, CA 92093